Clean Techn Environ Policy (2016) 18:171–184
DOI 10.1007/s10098-015-1004-z

ORIGINAL PAPER

Clean technology approach for the competitive binding of toxic metal ions onto MnO_2 nano-bioextractant

Martins O. Omorogie[1,3] · Jonathan O. Babalola[2] · Emmanuel I. Unuabonah[3,4] · Jian R. Gong[1]

Received: 16 October 2014 / Accepted: 30 June 2015 / Published online: 7 July 2015

Abstract The competitive extraction of Cr(III) onto *Nauclea diderrichii* seed epicarp doped with MnO_2 nanoparticles (MnO_2 nano-bioextractant (MNB)) in a single and binary batch system was studied. For validity of experimental data, chi square test, root mean square error, sum of the square errors, hybrid fractional error function, Marquart's percent standard deviation and standard absolute error were used. Among the kinetic models used, pseudo-second-order and Langmuir equations gave the best fits for the experimental data, with q_e (mg g) for the uptake of Cr(III) in single metal system onto MNB, then Cr(III) with Cd(II), Pb(II), Hg(II), KCl and $CaCl_2$ in binary metal systems onto MNB were 2.611, then 1.989, 1.016, 2.208, 1.249 and 1.868 from kinetic standpoint, respectively. The initial sorption rates, h (mg/g/min), and half lives, $t_{1/2}$ (min), for the uptake of Cr(III) in single metal system onto MNB, then Cr(III) with Cd(II), Pb(II), Hg(II), KCl and $CaCl_2$ in binary metal system onto MNB were 3.497, then 2.311, 2.274, 0.242, 2.956, 45.568 and 0.747, then 5.769, 1.766, 12.144, 1.762, and 2.415, respectively. Physicochemical surface analyses such as pH of point of zero charge, Brunauer–Emmett–Teller single point and multipoint techniques for surface area analyses, scanning electron microscopy and transmission electron microscopy were done on MNB and MnO_2 nanoparticles in order to understand their surface microstructures. Desorption study showed that MNB can be recycled and used for future study. Hence, MNB showed good potential to remediate Cr(III) from wastewaters and polluted water.

Keywords *Nauclea diderrichii* · Nano-bioextractant · Doping · Kinetics · Mass transfer

List of symbols

k_f	Freundlich constant $(L/mg)^{1/n}(mg/g)$
n_f	Empirical constant that represents the adsorption affinity
q_{max}	q_e for monolayer saturation (mg/g),
K_L	Langmuir adsorption constant (L/mg)
R_L	Dimensionless constant separation factor for equilibrium parameter
b_T	b_T heat of adsorption constant, which is related to K_T
K_T	Temkin equilibrium binding constant in (L/mg)
R	Universal gas constant, which is 8.314 (J/mol)
T	Absolute temperature in Kelvin
ε	Polanyi potential which is equal to $RT\ \mathrm{In}(1 + 1/C_e)$
q_m	Theoretical monolayer saturation capacity (mg/g)
$\theta = (1 - C_e/C_0)$	The degree of surface coverage

✉ Martins O. Omorogie
omorogiem@run.edu.ng; osaigbovoohireimen@gmail.com

✉ Jian R. Gong
gongjr@nanoctr.cn

[1] Laboratory for Nanodevices, National Center for Nanoscience and Technology-Chinese Academy of Sciences (NCNST-CAS), 100190 Beijing, People's Republic of China

[2] Biophysical Chemistry Unit, Department of Chemistry, University of Ibadan, Ibadan 200284, Nigeria

[3] Environmental and Chemical Processes Research Laboratory, Department of Chemical Sciences, Redeemer's University (RUN), P.M.B. 230, Ede, Osun State, Nigeria

[4] Institüt fur Chimie, Universität Potsdam, 14476 Potsdam, Germany

K_{FH}	Flory–Huggins model equilibrium constant
n_{FH}	Flory–Huggins model exponent
Q_B	Amount of solute adsorbed in forming a complete monolayer (mg/g)
K_B	BET constant that represents the energy of interaction with the surface
C_s	Saturation concentration of solute (mg/L)
E	Mean adsorption energy (kJ/mol)
A	Harkins–Jura constant
B	Harkins–Jura equilibrium constant
$\Delta G^0 = -RT \ln K_{FH}$	The Flory–Huggins Gibbs free energy of spontaneity (kJ/mol)

Introduction

Chromium pollution problem serves as one of the most serious toxic metal pollution in the globe, which has attracted increasing attentions of researchers due to vast advancement in global trends of advancements (Jacobs and Testa 2004). To a large extent, toxic metals have threatened the existence of man, terrestrial and aquatic biota, and thus hamper ecological sustainability. It is well known that chromium compounds are widely used in various industries, such as leather tanning, paints and pigments, mining, electroplating, steel fabrication, etc. The industrial wastewater from these processes holds a colossal amount of chromium pollutant that is harmful for ecological system and human health. Researchers have reported that exposure to certain level of chromium is responsible for lung cancer, chrome ulcers, nasal septum perforation, as well as brain damages (Chen et al. 2009; Bayramoglu and Arica 2008). Various research studies have shown that toxic metal ions can be removed from aqueous solutions by adsorption process in batch or continuous operation at laboratory scale, which can be considered to be ideal for large-scale treatment of effluents containing heavy metals at industrial scale (Garcia-Reyes and Rangel-Mendez 2010).

Adsorption of Cr(III) pollutants has been studied using various biomasses. Most of these biomasses (natural adsorbents that are mostly cellulosic based) are very attractive, cost effective, relatively abundant and ubiquitous in the environment.

The emergence of biosorption made it possible for various lignocelluloses to be utilised for the removal of Cr(III) from effluents, such as palm flower (Elangovan et al. 2008), rice bran (Oliveira et al. 2005), saltbush leaves (Sawalha et al. 2006), hazelnut shell (Cimino et al. 2000), *Agave lechuguilla* (Romero-Gonzalez et al. 2005), *Leersia hexandra* (Li et al. 2009), *Cassia fistula* and pretreated *C. fistula* (Abbas et al. 2008), *Opuntia ectodermis* (Barrera et al. 2006), *Citrus reticulata* (Zubair et al. 2008), etc.

Nauclea diderrichii (De wild) is a deciduous tree which thrives excellently in tropical rain forest areas of West and East Africa. It is a hard wood with good strength as a timber, and its resistance to termites makes it essentially valuable to the furniture, art, building and construction industries in West Africa. It is produced in large commercial scale, which is in hundreds of tonnes annually. It is found abundantly in Ibadan, Lagos, Akure, Benin City, Port Harcourt, Calabar and other parts of Southern Nigeria (Adeoye and Waigh 1983).

The bark is known to be used locally in the treatment of gonorrhoea, stomach pains, fever and sometimes diarrhoea. The extraction of secoiridoid and triterpenic acids from the stems of *N. diderrichii* has been reported (Adeoye and Waigh 1983).

Abundant amount is also found in Sierra Leone, Liberia, Togo, Cote d'ivoire, Ghana, Senegal, Burkina Faso and other West African countries (IUCN 1998); hence, the biomass from the epicarp of the seeds of this plant is thrown away, and this increases pollution in the environment. This makes it readily available in sawmills and forest research institutes where its seedlings are grown.

Adsorption of trace heavy metals by manganese oxides has been investigated intensively for a long time (Posselt et al. 1968; Johnson 1990). It has been shown that manganese oxides adsorb trace heavy metals more strongly than most other adsorbents (Johnson 1990). Studies have indicated that manganese dioxide has been used as adsorbent for the removal of heavy metals from aqueous solutions due to its selectivity. Apart from its ability to uptake heavy metals, manganese dioxide is also considered to be an economical, eco-friendly and easily available adsorbent in the environment (Subramaniam et al. 2008).

Researchers have shown that nanomaterials are highly promising in water purification process due to their unique properties like ease with which they can be anchored onto solid matrices and the flexibility to functionalise them with different functional groups, to enhance their affinities towards target molecules (Tripathy et al. 2006; Zou et al. 2006; Subramaniam et al. 2008; Lisha et al. 2010; Shi et al. 2011).

Various nanoparticles have been used in adsorbing heavy metals from aqueous solutions including MnO_2 nanowhiskers for the removal of Hg(II) (Lisha et al. 2010), titanate nanotubes for the removal of Pb(II) and Cd(II) (Xiong et al. 2011), amino-functionalised mesoporous silica for the removal of Cu(II), Ni(II), Pb(II), Cd(II) and Zn(II) (Aguado et al. 2009), zero-valent iron nanoparticles

for the remediation of Cr(VI) (Melitas et al. 2001), iron and iron oxide nanoparticles for the removal of Cr(VI) (Ĺopez-Ťellez et al. 2011), carbon nanotubes for Cr(VI) (Tsai et al. 2011) and mesoporous silica nanoparticles for the removal of Hg(II), Cd(II), Pb(II), Cu(II), Ag(I) and Cr(VI) (Shi et al. 2011).

Recently, some of the adsorbents that have been used to adsorb Cr(III) from aqueous solutions are *Termitomyces clypeatus* (Fathima et al. 2015), *Parkia biglobosa* chaff and pulp (Ogbodu et al. 2015), immature coal (Lao-Luque et al. 2014), nanocrystalline cellulose (Kiran et al. 2014), *Sargassum cymosum* (De Souza et al. 2013), chitosan polymer (Zuo and Balasubramanian 2013), sugarcane biochar and pulp residue (Xiong et al. 2013), *Bacillus subtilis* (Aravindhan et al. 2012), among others.

In our previous treatise, Omorogie et al. (2012) studied the adsorption of Cr(III) by *N. diderrichii* seed waste. This study showed that *N. diderrichii* seed waste could not stay long in aqueous solutions when subjected to adsorption processes. This was due to its low bulk density, low resistant to water or solutions during experiments and degradation potential. It easily degrades when subjected to end use, thus, limiting its end use to small scale. An attempt to overcome these drawbacks, led to the use of MnO_2 nanoparticles as dopant for *N. diderrichii* seed waste, thereby producing a new material. This modification will make the *N. diderrichii* seed waste suitable for large- or industrial-scale applications.

This study highlights the use of MnO_2 nanoparticles-doped *N. diderrichii* bioextractant (MNB) in sequestering of Cr(III) ion from aqueous solution. This study further considers the kinetic dynamics, equilibrium and thermodynamics of the adsorption system.

Materials and methods

Preparation of *Nauclea diderrichii* seed biomass

Nauclea diderrichii seed epicarp (biomass) was obtained from the Forest Research Institute of Nigeria (FRIN), in Ibadan (7°23′16″N, 3°53′47″E), Nigeria, West Africa. After collection, these seed wastes were dried in an oven at 60 °C for 3 h. Thereafter, they were pulverised into very small size. The adsorbent was later sieved to 450-μm particle size (possesses better solid–liquid phase separation than 150 and 300 μm) which was used in this research.

Hydrothermal synthesis of MnO_2 nanoparticles and MNB

The MnO_2 nanoparticles were synthesised by hydrothermal technique (Oszlanczi 2011). Sixty millilitres of 0.1 M of $KMnO_4$ precursor was added to 10 mL ethylene glycol. This reaction mixture was thoroughly stirred in an ultrasonicator (KQ-300E Chinese Model) at 298 K for 3 h. Thereafter, 40 mL of the reaction mixture was introduced into Teflon-lined autoclave, then placed in an oven (DHG-9030A Chinese Model) for 16 h at 200 °C and was allowed to cool to room temperature. After cooling, a suspension of brown particles at the bottom of the Teflon-lined autoclave was formed. This suspension was homogenised, and a brown solution was obtained. Ten millilitres of this brown solution was filtered using filter paper, and the brown residue further obtained was dried in an oven for 6 h at 100 °C. The brown powder (MnO_2 nanoparticles) obtained was taken for characterisation using transmission electron microscopy (TEM). Thereafter, 30 mL of this brown solution was transferred to a 150-mL beaker, to which accurately weighed amount of *N. diderrichii* seed epicarp (biomass) was added. The resultant slurry was stirred for 24 h continuously at room temperature at 1200 rpm.

The resultant slurry was filtered and its wet residue, the MNB, was dried in an oven for 6 h at 100 °C and kept in an airtight low-density polyethylene bags for use.

Physicochemical analyses of MnO_2 nanoparticles and MNB surfaces

The surfaces of MnO_2 nanoparticles and MNB were characterised using scanning electron microscopy (SEM) (Hitachi S4800 model) and TEM, F20 S-TWIN transmission electron microscope (Tecnai G2, FEI Co.), at 200 kV accelerating voltage were used to consider the surface morphology of the adsorbent prepared. The X-ray diffraction (XRD) analysis was also done using the XRD D/Max-2500 (Rigaku, Japan) with Cu K α radiation, $\lambda = 1.5406$ nm. The N_2 sorption-desorption analysis was carried using Brunauer–Emmett–Teller (BET) specific surface area analyser, Micromeritics Instrument Corporation, ASAP 2020 Model analyser (for specific surface area measurement). The pH at the point of zero charge (pHpzc), was determined using the solid addition method as reported by Stumm and Morgan (1996).

Adsorption studies

Fifty milligrammes of MNB was weighed into 3-mL airtight plastic containers.

The single metal stock solutions containing 1000 mg/L of Cr(III) were prepared by dissolving accurately weighed amounts of $Cr(NO_3)_3{\cdot}9H_2O$ (Beijing Chemical Works Company, China) in de-ionised water prepared by the Milli-Q water deionizer.

Also, stock solutions of 1 M KCl and I M $CaCl_2$ were prepared by dissolving accurately weighed amounts of KCl

and $CaCl_2$ in de-ionised water prepared by the Milli-Q water deionizer.

Each binary metal stock solution containing (1000/250) mg/L of Cr(III)/Cd(II), Cr(III)/Pb(II) and Cr(III)/Hg(II) was prepared by dissolving accurately weighed amounts of $Cr(NO_3)_3.9H_2O$, $Cd(NO_3)_2.4H_2O$, $Pb(NO_3)_2$ and $Hg(NO_3)_2.½H_2O$ (Beijing Chemical Works Company, China) in de-ionised water prepared by the Milli-Q water deionizer.

Also, each binary stock solution containing (1000 mg/L/1 M) each of Cr(III)/KCl and Cr(III)/$CaCl_2$ was prepared by dissolving accurately weighed amounts of $Cr(NO_3)_3.9H_2O$, KCl and $CaCl_2$ (Beijing Chemical Works Company, China) in de-ionised water prepared by the Milli-Q water deionizer.

Various experimental solutions were further prepared by diluting the stock solutions above to the desired working concentrations when needed.

For kinetic study (single system), 50 mg of MNB was added to 20 mg/L of Cr(III) and then agitated with a thermostatic shaker (THZ-C Chinese Model) at 125 rpm for 0.5–120 min at 303 K.

For equilibrium study (single system), 50 mg of MNB was added to 20–100 mg/L of Cr(III), agitated at 125 rpm for 120 min at 303 K.

For thermodynamic study (single system), 50 mg of MNB was added to 20 mg/L of Cr(III) and then agitated with a thermostatic shaker (THZ-C Chinese Model) at 125 rpm for 120 min at 303–333 K, respectively.

The effect of competitive ions and electrolytes on the adsorption of Cr(III) onto MNB (binary system) was investigated by adding 50 mg of MNB to a set of 100-mL conical flasks containing (20/5) mg/L of Cr(III)/Cd(II), Cr(III)/Pb(II) and Cr(III)/Hg(II), then (20 mg/L/0.01 M) of Cr(III)/$CaCl_2$ and Cr(III)/KCl agitated with a thermostatic shaker (THZ-C Chinese Model) at 125 rpm for 120 min at 303 K.

At equilibrium, the suspensions were filtered using 0.45 μm filter papers, and aliquots of the pure supernatant liquids were collected for the analysis of residual Cr(III) ion concentration in the aqueous solutions using ICPE 9000 Shimadzu Model of ICP-AES (Inductively Coupled Plasma-Atomic Emission Spectrometer).

The amount of Cr(III) ion in the aqueous solutions adsorbed by MNB was calculated by difference using the following equation:

$$q_e = \int_{i=1}^{n} \left(\frac{(C_o - C_e)\ V}{W} \right), \quad (1)$$

where i is the number of experimental data points, n is the maximum experimental data point,C_o is the initial concentration of Cr(III) ion in the aqueous solutions (mg/L), C_e is the equilibrium concentration of residual Cr(III) ion in the aqueous solutions (mg/L), V is the volume of the aqueous solutions containing Cr(III) ion (L), W is the weight of adsorbent (g) and q_e is the amount of Cr(III) ion adsorbed by the adsorbent (mg/g).

After adsorption experiment, Cr(III)-loaded MNB samples were dried in an oven for 2 h at 70 °C. Thereafter, 50 mg each of the dried Cr(III)-loaded MNB was weighed and added to 20 mL of 0.01 and 0.1 M each of H_2SO_4 and HCl desorbents in 100-mL conical flasks. The suspensions obtained were agitated for 2 h in a thermostatic shaker (THZ-C Chinese Model) at 125 rpm. At equilibrium, pure supernatants were obtained using filter papers, and these supernatants were taken for analysis using ICPE 9000 Shimadzu Model of ICP-AES (Inductively Coupled Plasma-Atomic Emission Spectrometer) to get the amount of Cr(III) desorbed from the adsorbents, and % desorption was calculated using the following equation:

$$\%\ \text{Desorption} = \frac{\text{Amount desorbed (mg/L)}}{\text{Amount adsorbed (mg/L)}} \times \frac{100}{1}. \quad (2)$$

Theory of models

Kinetic modelling

To understand the time dynamics of these adsorption processes as they concern the controlling mechanism of adsorption process such as chemical reaction, mass transfer and diffusion control (Ho 1995). The residence time of adsorbate plays a paramount role for the adsorption rate due to its effect on the solid-liquid interface (Ho 1995).

The pseudo-second-order kinetic model assumes that chemical sorption of the adsorbate takes place on the adsorbent (Sevim et al. 2011; Ho et al. 2005). It has been proposed that adsorption comprises three steps (Onal et al. 2007).

Firstly, the diffusion of adsorbate through the solution to the external surface of the adsorbent or the boundary layer diffusion of the solute molecules.

Secondly, the gradual adsorption step, in which intra-particle diffusion may be rate limiting.

Thirdly, the diffusion of adsorbate particles to adsorption sites either by pore diffusion through the liquid-filled pores or by a solid diffusion mechanism (Onal et al. 2007; Gerente et al. 2007).

The initial sorption rates (mg/g/min) and half lives (min) of the adsorption system are calculated using $h = K_2 q_e^2$ and $t_{0.5} = \frac{1}{K_2 q_e}$, respectively, where K_2 (g/mg/min) and q_e (mg/g) are the pseudo-second-order rate constant and the amount of metal ion adsorbed at equilibrium, respectively.

Morris–Weber intraparticle diffusion model gives an understanding of the mass transfer of the solute molecules (adsorbate) from the bulk liquid phase to the external surface of the solid (adsorbent), the rate limiting step of the process, and the thickness of the boundary layer during the process (film diffusion) (Gerente et al. 2007). The experimental data obtained were fitted into intraparticle diffusion model (Gerente et al. 2007; Ofomaja et al. 2009).

Elovich kinetic model is applicable to adsorbent having heterogeneous binding sites, and difference in activation energies occurs during the adsorption of toxic heavy metals (Ofomaja et al. 2009). Tables 1, 2, 3 and 4 show the linearised forms, parameters and error function values of the various kinetic models.

Equilibrium and thermodynamic modellings

The optimization design for adsorption system involves the modelling of the experimental data obtained for the removal of Cr (III) ions from aqueous solution by MNB. It is therefore significant and noteworthy to establish the most appropriate correlation curves for the equilibrium data got; hence, seven isotherm models that were used to analyse equilibrium data (Ofomaja et al. 2009). They are Freundlich (Freundlich 1906) (Eq. 3), Langmuir (Langmuir 1916) (Eq. 4), Temkin (Temkin and Pyzchev 1939) (Eq. 6), Dubinin-Radushkevich (Dubinin 1960) (Eq. 7), Harkins-Jura (Harkins and Jura 1944) (Eq. 8), Flory–Huggins (Horsfall and Spiff 2005) (Eq. 9) and Brunauer–Emmett–Teller [BET] (Brunauer et al. 1938) (Eq. 10). The linear forms of these equations are.

$$\ln\ q_{\mathrm{e}}\ =\ \ln\ K_{\mathrm{f}}\ +\ \frac{1}{n_{\mathrm{f}}}\ln\ C_{\mathrm{e}}, \tag{3}$$

$$\frac{C_{\mathrm{e}}}{q_{\mathrm{e}}} = \frac{1}{K_{\mathrm{L}} q_{\max}}\ +\ \frac{C_{\mathrm{e}}}{q_{\max}} \tag{4}$$

$$R_{\mathrm{L}} = \frac{1}{1 + K_{\mathrm{L}} C_0}, \tag{5}$$

$$q_{\mathrm{e}} = b_{\mathrm{T}} \ln K_{\mathrm{T}} + b_{\mathrm{T}} \ln C_{\mathrm{e}}, \tag{6}$$

$$\ln\ q_{\mathrm{e}}\ =\ \ln\ q_{\mathrm{f}}\ -\beta\varepsilon^2 \tag{7}$$

Table 1 Description of different error functions

Error function	Definition/expression
Chi square test (CST)	$\chi^2 = \sum_{i=1}^{n} \frac{\left(q_{\mathrm{e,exp}} - q_{\mathrm{e,calc}}\right)^2}{q_{\mathrm{e,calc}}}$
Root-mean square error (RMSE)	$\sqrt{\frac{1}{n-2}\sum_{i=1}^{n}\left(q_{\mathrm{e,exp}} - q_{\mathrm{e,calc}}\right)^2}$
Sum of the square of errors (SSE)	$\sum_{i=1}^{n}\left\{q_{\mathrm{e,calc}} - q_{\mathrm{e,exp}}\right\}_i^2$
Hybrid fractional error function (HYFEF)	$\frac{100}{n-m}\sum_{i=1}^{n}\left[\frac{\left(q_{\mathrm{e,exp}} - q_{\mathrm{e,calc}}\right)^2}{q_{\mathrm{e,exp}}}\right]_i$
Marquart's percent standard deviation (MPSD)	$100\left(\sqrt{\frac{1}{n-m}\sum_{i=1}^{n}\left[\frac{q_{\mathrm{e,exp}} - q_{\mathrm{e,calc}}}{q_{\mathrm{exp}}}\right]_i^2}\right)$
Sum of absolute errors (SAE)	$\sum_{i=1}^{n}\left\lvert q_{\mathrm{e,calc}} - q_{\mathrm{e,exp}}\right\rvert$

m number of parameters of the isotherm equation, n number of data points, $q_{\mathrm{e,calc}}$(mg/g) is the equilibrium capacity obtained by calculating from the model and $q_{\mathrm{e,exp}}$ is the equilibrium capacity of experimental data (mg/g)

Table 2 Adsorption kinetic models, their linearised forms and description of their parameters

Kinetic models	Equations	Linearised forms	Plots	Parameters
Pseudo-second order	$\frac{\mathrm{d}q_t}{\mathrm{d}t} = K_2(q_{\mathrm{e}} - q_t)^2$	$\frac{t}{q_t} = \frac{1}{K_2 q_{\mathrm{e}}^2} + \frac{t}{q_{\mathrm{e}}}$	$\frac{t}{q_t}$ *Vs* t	$q_e = (\mathrm{slope})^{-1}$ $K_2 = (\mathrm{slope})^2 \big/ \mathrm{intercept}$
Weber–Morris intraparticle diffusion	$\frac{\mathrm{d}q_t}{\mathrm{d}t^{-1/2}} = K_\alpha$	$q_t = K_\alpha t^{1/2} + C$	q_t *Vs* $t^{1/2}$	$K_\alpha = \mathrm{slope}$ $C = \mathrm{intercept}$
Elovich	$\frac{\mathrm{d}q_t}{\mathrm{d}t} = \alpha \exp(-\beta q_t)$	$q_t = \frac{1}{\beta}\ln(\alpha\beta) + \frac{1}{\beta}\ln t$	q_t *Vs* $\ln t$	$\beta = (\mathrm{slope})^{-1}$ $\alpha = (\mathrm{slope}) \exp\left(\frac{\mathrm{intercept}}{\mathrm{slope}}\right)$

Table 3 Effects of competing ions and electrolytes on adsorption kinetic parameters for the uptake of Cr(III) ion by MNB

Kinetic models	MNB	5(mg/L) Cd(II)	5 (mg/L) Pb(II)	5 (mg/L) Hg(II)	0.01 M KCl	0.01 M $CaCl_2$
Pseudo-second order						
R^2	0.998	0.999	0.997	0.925	0.999	0.999
K_2 (g mg/min)	0.513	0.013	0.141	0.028	0.109	0.128
q_e (mg/g)	2.611	1.989	1.016	2.208	1.249	1.868
h(mg/g/min)	3.497	2.311	2.274	0.242	2.956	45.568
$t_{1/2}$ (min)	0.747	5.769	1.766	12.144	1.762	2.415
Morris–Weber intraparticle diffusion						
R^2	0.655	0.582	0.809	0.929	0.778	0.492
K_{MW}(mg/g/min$^{1/2}$)	0.383	0.075	0.249	0.340	0.192	0.053
C	2.966	2.208	3.092	0.225	3.018	5.485
Elovich (R^2)	0.944	0.779	0.832	0.788	0.986	0.587
α (mg/g min)	2.820	2.019	2.165	1.114	2.085	3.026
β (g/mg)	1.221	6.452	2.174	1.730	2.564	7.813

Table 4 Adsorption kinetics error function values for the uptake of Cr(III) ion from aqueous solutions by MNB

	CST	*RMSE*	*SSE*	*HYFEF*	*MPSD*	*SAE*
Pseudo-second order						
MNB	26.492	8.016	64.125	153.975	9.360	23.494
5 (mg/L) Cd(II)	39.423	52.107	416.857	1932.013	13.928	51.995
5 (mg/L) Pb(II)	10.171	2.059	16.473	54.775	3.593	11.337
5 (mg/L) Hg(II)	3.106	1.321	2.568	16.538	1.097	2.589
0.01 M KCl	2.975	1.690	5.520	22.000	1.051	1.568
0.01 M $CaCl_2$	73.498	161.048	1288.383	283.488	25.967	110.790
Morris–Weber intraparticle diffusion						
MNB	88.645	11.755	94.041	258.650	1.801	29.645
5 (mg/L) Cd(II)	291.176	6.135	49.076	244.225	2.787	22.081
5 (mg/L) Pb(II)	174.989	12.088	96.707	299.875	2.186	30.904
5 (mg/L) Hg(II)	1.074	0.156	1.244	8.475	1.249	2.242
0.01 M KCl	205.637	11.506	92.045	306.250	2.377	30.196
0.01 M $CaCl_2$	2613.835	37.696	301.564	660.300	3.277	54.873
Elovich						
MNB	2.577	6.967	55.738	143.588	1.910	22.567
5 (mg/L) Cd(II)	6.297	5.022	40.175	197.550	2.225	19.928
5 (mg/L) Pb(II)	4.709	9.883	79.065	236.213	1.664	27.791
5 (mg/L) Hg(II)	1.387	1.281	2.251	9.788	1.137	1.137
0.01 M KCl	4.997	8.961	71.684	233.038	1.765	26.572
0.01 M $CaCl_2$	8.400	34.226	273.806	598.788	2.968	52.273

$$\frac{1}{q_{e^2}} = \left(\frac{B}{A}\right) - \left(\frac{1}{A}\right) \ln C_e, \tag{8}$$

$$\log \theta/C_0 = \log K_{FH} + n_{FH} \log(1-\theta), \tag{9}$$

$$\frac{C_e}{(C_s - C_e)q_e} = \frac{1}{K_B Q_B} + (K_B - 1)\frac{C_e}{Q_E K_B C_s}. \tag{10}$$

All the constants for the equilibrium isotherms are defined in the nomenclature list provided.

In order to understand the impact of temperature, the heat dynamics, spontaneity and feasibility of an adsorption system, there is need to calculate and evaluate the various thermodynamic parameters of this process.

Clausius Clapeyron provided basic mathematical equations for obtaining thermodynamic parameters from adsorption data (Young and Crowell 1962).

The differential form of the Clausius Clapeyron equation is given as follows:

$$\frac{\mathrm{d}\ln K_{\mathrm{FH}}}{\mathrm{d}T} = \frac{\Delta H^0}{RT^2}. \tag{11}$$

Integration and rearrangement will give

$$\int \frac{\mathrm{d}\ln K_{\mathrm{FH}}}{\mathrm{d}T} = \int_0^T \frac{\Delta H^0}{RT^2},$$

$$\int \mathrm{d}\ln K_{\mathrm{FH}} = \frac{\Delta H^0}{R}\int_0^T \frac{\mathrm{d}T}{T^2},$$

$$\ln K_{\mathrm{FH}} = -\frac{\Delta H^0}{RT} + Y.$$

Recall $\Delta G^0 = -RT\ln K_{\mathrm{FH}}$ and $\Delta G^0 = \Delta H^0 - T\Delta S^0 \therefore -RT\ln K_{\mathrm{FH}} = \Delta H^0 - T\Delta S^0$,

$$\ln K_{\mathrm{FH}} = \frac{\Delta S^0}{R} - \frac{\Delta H^0}{RT}. \tag{12}$$

where ΔH^0, ΔS^0, R and T are enthalpy (kJ/mol), entropy (J/mol/K), the universal gas constant which is 8.314 J/mol/K and the temperature (K), respectively.

Results and discussion

Microstructural characterisations of MnO_2 nanoparticles and MNB surface

Effect of pHpzc

The microstructural characterisations of *N. diderrichii* seed epicarp were reported by Omorogie et al. (2012) in our previous treatise.

The pHpzc is the pH at which the amount of negative charges on the adsorbent surface is equal to the amount of positive charges. This is also the pH at which there is net zero charge on the surface of the adsorbent when adsorption has not taken place. The organic functional groups on the adsorbent surface may acquire a negative or positive charge depending on the solution pH. At pH values higher than the pHpzc, the sites are mainly in dissociated form and acquire a negative charge, while at pH values lower than the pHpzc of these groups, the sites will be in the associated form with a proton to become positively charged (Li et al. 2007). The pHpzc of MNB was 4.77. This result showed that <pH 4.77, small amount of Cr(III) would be adsorbed by MNB and >pH 4.77, large amount of Cr(III) would be adsorbed by MNB. In other words, the adsorption of Cr(III) onto MNB would be favoured at pH above 4.77. The merit of this pHpzc value lies in the fact that the adsorption of Cr(III) would predominantly take place over a short pH range, rather than a long pH range as it is observed with most biomasses. The advantage of adsorption taking place over a short pH range is the limitation of complex formation through complexation and precipitation, with the ability to block the active sites on the surface of the adsorbent (Li et al. 2007; Onal et al. 2007). At pH 6.5, the change in the pH began to drop as a result of the sharp decrease in the negatively charged functional groups binding to the cations. This decrease became more significant as the initial pH increased towards 12.0. Figure 1 shows the pictorial representation of the pHpzc for MNB.

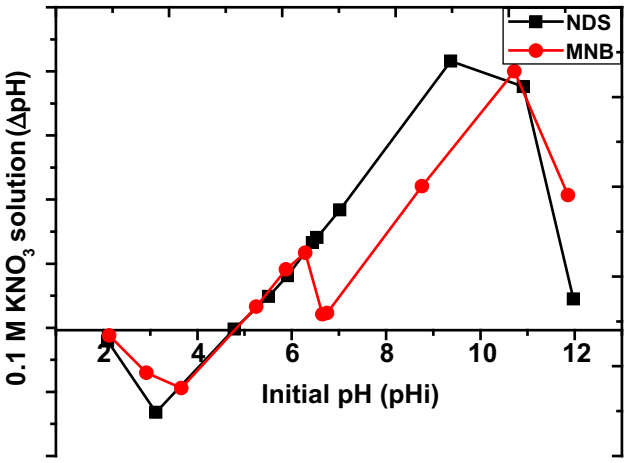

Fig. 1 The pHpzc of MNB using 0.1 M KNO_3 solution

Scanning electron microscopy (SEM) and transmission electron microscopy (TEM) and Brunauer–Emmett–Teller(BET) multi-point specific surface area analysis

The SEM has been widely used for the analysis of the surface microstructures and micro-area compositions of adsorbents with an aim to understand their pore structures and morphologies, which play significant roles in sorption process. Figure 2 shows the SEM images of the unloaded MNB and Cr(III)-loaded MNB. These images revealed that MNB and Cr(III)-loaded MNB have their morphologies with scanty and scattered pores of various lump sizes that are irregularly shaped on their surfaces. The MnO_2 nanoparticles were made up of tiny grainy ball-like particles. Also, Fig. 2 depicts TEM images of MnO_2 nanoparticles at 20 nm.

The BET multi-point surface area gives an understanding of the surface coverage ability of an adsorbent that can be filled with adsorbate(s). The BET multi-point surface area decreased from 5.36 m^2/g in *N. diderrichii* seed epicarp to 1.25 m^2/g in MNB. Also, the BET multi-point surface area of MnO_2 nanoparticles was 19.32 m^2/g. Although the surface for MNB was lower to that of *N. diderrichii* seed epicarp, MNB has arrayed pores that were

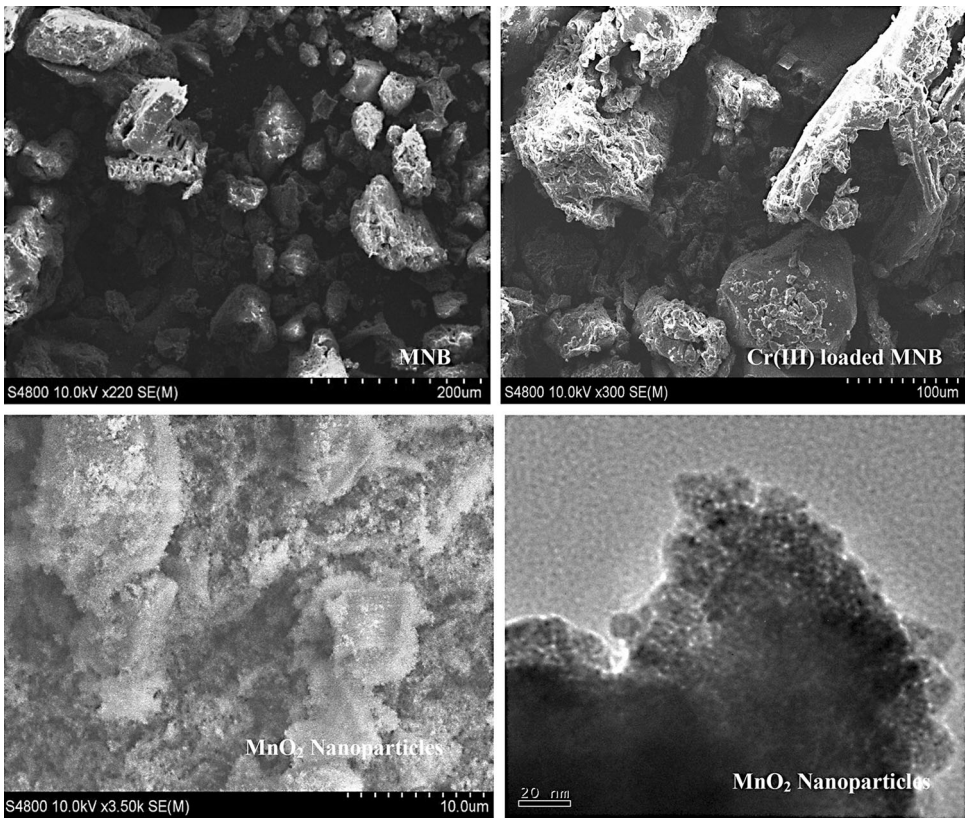

Fig. 2 SEM micrographs of MNB, Cr(III) loaded MNB, MnO_2 nanoparticles and TEM micrographs of MnO_2 nanoparticles

absent in *N. diderrichii* seed epicarp. These arrayed pores in MNB were present due to the modification of *N. diderrichii* seed epicarp with MnO_2 nanoparticles.

X-ray diffraction (XRD) analysis

XRD diffractograms of MNB and the Cr(III) loaded MNB are shown in Fig. 3.

The XRD gives information about the change(s) in the crystalline and amorphous portions of MNB and the Cr(III)-loaded MNB. Cr(III)-loaded MNB showed a characteristic peak intensity at $2\theta = 20.7°$, and the MNB showed very low peak intensity at $2\theta = 21.3°$. It shows that the MNB adsorbent has a crystal structure with low interlayer distance, which is attributed to the presence of MnO_2 (Thirumavalavan et al. 2011; Granados-Correa et al. 2011). After MNB was used for adsorption, its peak intensity was virtually retained which suggests that there was no collapse in the crystal structure of the MNB, which further attributes the presence of Cr(III) ions on its surface.

Adsorption kinetics, equilibrium and thermodynamics

The adsorption kinetics of Cr(III) onto *N. diderrichii* seed epicarp was reported by Omorogie et al. (2012) in our previous treatise.

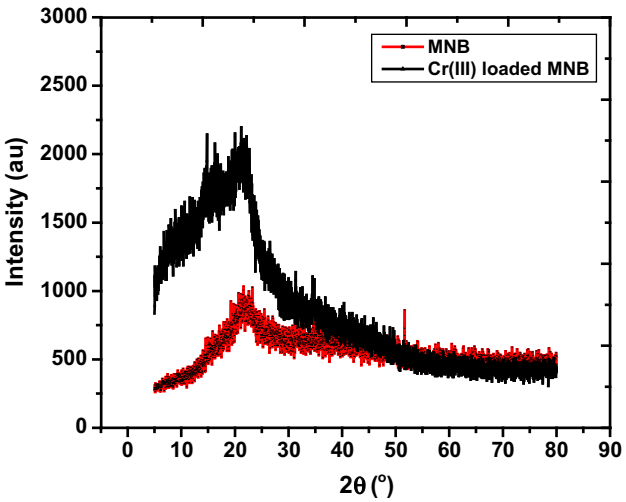

Fig. 3 XRD diffractograms of MNB and Cr(III) loaded MNB

The experimental data best fit the pseudo-second-order kinetic model with the highest correlation co-efficients $R^2 > .925$, which is greater than those obtained from Morris–Weber intraparticle diffusion and Elovich models. The pseudo-second-rate constants K_2, the theoretical q_e, the initial sorption rates h and half lives of the reactions $t_{1/2}$ for single adsorption system of MNB were 0.513 g/mg/min, 2.611 mg/g, 3.497 mg/g/min and 0.747 min, respectively.

Similarly, the pseudo-second rate constants K_2, the theoretical q_e, the initial sorption rates h and half lives of the reactions $t_{1/2}$ for competitive adsorption system are in the range of 0.013–0.141 g/mg/min, 1.016–2.208 mg/g, 0.242–45.568 mg/g/min and 1.762–12.144 min, respectively.

The implication of this result is that the pseudo-second-order rate constant and the initial sorption rates for the single adsorption system were less than those of the competitive adsorption system due to the fact that the metal ions were competing for the active sites that were available for MNB to bind to. There was a stiff competition among Cr(III) and the other metal ions for the functional moieties on the surface of the adsorbents. This eventually led to a decrease in the pseudo-second-order rate constant and initial sorption rate of Cr(III) adsorption. Moreover, this stiff competition also led to a decrease in the amount of Cr(III) adsorbed.

Kinetically, for the competitive adsorption of Cr(III)/Ca, Cr(III)/Cd(II) and Cr(III)/Hg(II) onto MNB tend to show higher initial sorption rates, h(mg/g/min) than those of Cr(III)/K, Cr(III)/Pb(II). This might be due to the fact that Ca, Cd(II) and Hg(II) possess ionic radii that are smaller than those of K and Pb(II). The lower the ionic radius of a metal ion, the more readily it looses its hydration shell (Mobasherpour et al. 2012; Şahan and Öztürk 2014; Venkatesan et al. 2014; Rodríguez-Martínez et al. 2015). For all the competitive ions, the values of the initial sorption rates of K and Ca were higher than others due to their solubility and ease of ionisation water when compared to toxic metals. Also, the values for the pseudo-second order rate constants, K_2 (g/mg/min), for the competitive adsorption of Cr(III)/Cd(II) and Cr(III)/Hg(II) onto MNB were smaller than those of others. This also buttressed the fact that these adsorption processes were kinetically faster than others. It is interesting to note that the adsorption capacity, q_e(mg/g) of the uptake of Cr(III) by MNB slightly decreased due to the presence of competing ions and electrolytes thereby limits its binding to the functional moieties on the surface of MNB. Interestingly, this study has revealed that the higher the competing ions in the solution, the lower the amount of target ions that will bind to the adsorbent. The competitive adsorption study is very relevant to situations when the pollutant matrix of potable water source or industrial wastewaters is laden with different toxic metal ions. The more complex the pollutant matrix is, the more difficult it is for the adsorbent remove the pollutants.

The Morris–Weber intraparticle diffusion constants K_α were obtained in the range of 0.022–0.383 for single and binary (competitive) adsorption processes. The constant C, which are measures of the thickness of the boundary layers/films of the adsorbents were found to be in the range of 0.225–5.941 for single and binary systems.

The implication of this is that the various linear plots did not pass through the origin; hence, the values of C are >0. This suggests that intraparticle diffusion was not the only rate controlling step in these adsorption processes. It was possible that film and pore diffusion also took part in the rate controlling or limiting steps of these adsorption processes (Lorenc-Grabowska and Gryglewicz 2005).

According to Kumar et al. (2009), there is also the possibility that the adsorption processes were initially controlled by intraparticle transport of metals by surface diffusion process, and later controlled by transport of metals by pore diffusion.

Elovich kinetic model gave constants α(mg/g min), which are the initial adsorption rate and β (g/mg), which is the Elovich constant that is related to the extent of surface coverage and the activation energy involved in chemisorption. The values of α and β were 1.114–3.720 and 1.221–21.277, respectively. The values of α and β also buttressed the fact that the adsorption of Cr(III) onto MNB was predominantly chemisorptive. Elovich equation also gave the smallest set of error function values with respect to the other kinetic models (see Tables 2, 3 and 4).

Omorogie et al. (2012) reported the adsorption of Cr(III) ion onto *N. diderrichii* seed epicarp was 5.57 mg/g at 20 mg/L initial Cr(III) ion concentration. At this same initial concentration, the adsorption of Cr(III) ion by MNB was obtained as 2.611 mg/g.

The adsorption of Cr(III) by MNB was lower than that of *N. diderrichii* seed epicarp due to low single crystals growth of MnO_2 nanoparticles during their hydrothermal synthesis (Byrappa and Yoshimura 2001). This also resulted in the disarray of the very small amount of single crystals formed. Hydrothermal technique with large growth of single crystals increases the surface area of nanomaterials (Byrappa and Yoshimura 2001). For instance, the single point and BET multi-point surface areas decreased from 2.53 and 5.36 m^2/g in *N. diderrichii* seed epicarp to 0.82 and 1.25 m^2/g in MNB, as the single point and BET multi-point surface areas of MnO_2 nanoparticles were 17.99 and 19.32 m^2/g.

The values of K_f and their error functions are relatively large at temperature of 303 K, but those obtained for 318 and 333 K were small. Also, the values for $1/n_f$ at 303–333 K were $\leq$2.78.

The experimental data obtained best fit the Langmuir isotherm because of the highest correlation co-efficients, R^2, which were $\leq$0.998 for 303–333 K, and small error function values which were got. The values of K_L at all temperatures were <1, which indicated that the adsorption system was favourable. The saturation monolayer adsorption capacities,

Table 5 Equilibrium model constants and error function values for the uptake of Cr(III) by MNB

Isotherms/parameters									
Freundlich	K_f $\{(L/mg)^{1/n}(mg/g)\}$	$1/n$		R^2	CST	RMSE	SSE	HYFEF	MPSD
303 K	3463.38	2.780		0.974	5.48E+7	6.48E+6	3.36E+14	2.44E+15	4.48E+15
318 K	8.415	0.200		0.974	16.615	4.774	182.340	354.625	156.335
333 K	7.846	0.140		0.970	4.454	2.257	40.759	75.563	31.726
Langmuir	K_L (L/mg)	q_{max} (mg/g)	R_L	R^2	CST	RMSE	SSE	HYFEF	MPSD
303 K	0.095	5.000	0.913	0.935	180.433	2.498	49.907	235.275	266.600
318 K	1.727	5.263	0.366	0.997	10.859	2.439	47.580	88.100	36.991
333 K	3.400	5.822	0.227	0.998	6.843	4.352	34.815	60.750	24.024
Temkin	K_T (L/mg)	b_T		R^2	CST	RMSE	SSE	HYFEF	MPSD
303 K	21.084	5.770		0.998	281.346	33.969	9231.171	54841.250	84009.299
318 K	483.21	1.330		0.982	11.109	3.723	110.880	215.575	95.002
333 K	3204.031	0.970		0.977	3.651	2.014	32.459	60.150	25.261
Dubinin-Radushkevich	β	q_m(mg/g)	E (kJ/mol)	R^2	CST	RMSE	SSE	HYFEF	MPSD
303 K	3.7E−6	8.415	0.367	0.961	1672.349	197.484	3.12E + 5	1.5E + 6	1.76E + 6
318 K	7.2E−8	5.312	2.635	0.933	0.012	0.099	0.079	0.155	0.067
333 K	3.9E−8	5.930	3.580	0.926	0.011	0.095	0.072	0.131	0.565
Harkins–Jura	A	B		R^2	CST	RMSE	SSE	HYFEF	MPSD
303 K	0.641	2.474		0.825	5.954	1.117	9.980	45.338	50.098
318 K	107.527	0.012		0.952	7.515	2.940	69.141	133.488	58.436
333 K	172.414	0.016		0.951	1.328	1.150	10.585	19.600	8.232
Flory–Huggins	K_{FH} (L/mg)	n_{FH}		R^2	CST	RMSE	SSE	HYFEF	MPSD
303 K	190.546	−2.780		0.974	680.110	83.842	56235.654	4.14E + 5	7.66E + 5
318 K	34.674	−0.200		0.974	129.757	19.946	3182.607	6111.413	2661.162
333 K	30.903	−0.130		0.970	115.629	18.459	2725.995	4922.475	2014.658
BET	K_B	Q_B (mg/g)		R^2	CST	RMSE	SSE	HYFEF	MPSD
303 K	146.921	0.064		0.840	4.34E + 6	891.628	6.36E + 6	4.34E + 7	7.56E + 7
318 K	1.0035	0.013		0.987	461.325	11.321	1025.354	1960.913	850.464
333 K	1.0013	0.006		0.992	410.358	10.645	906.562	1632.325	666.182

q_{max} for the uptake of Cr (III) MNB were ≤5.82 mg/g at 303–333 K (see Table 5).

The saturation monolayer adsorption capacities, q_{max} (mg/g) and K_L (L/mg) of Cr(III) onto MNB increased with increase in temperature. But the separation factor (a dimensionless constant), R_L, decreased with increase in temperature. This implied that the adsorption process was more favourable as temperature increased. This further means that the adsorption processes will be more favourable at elevated temperatures. Also, the Langmuir isotherm and the values of the error functions, when compared with those of the Freundlich isotherm showed that the surface of MNB predominantly comprise heterogeneous sites, thus, making the adsorption of Cr(III) by MNB to be of the monolayer form than the multilayer form. From this, it could be deduced that the mechanism of adsorption of Cr(III) by MNB is predominantly chemisorption, rather than physisorption (Lao-Luque et al. 2014; Ogbodu et al. 2015).

The error function values for the pseudo-second-order model were smaller than those of other kinetic models, and the error function values for Langmuir isotherm were also smaller than those of other isotherms. This clearly buttresses that the fact that chemisorptive binding of Cr(III) onto MNB culminated into the formation of monolayers.

For Temkin isotherm, the equilibrium binding constants b_T were obtained as ≤5.77 at 303–333 K.

For Dubinin-Radushkevich isotherm, its correlation coefficients R^2 values ≤0.97 as shown in Table 2. The error function values of Dubinin-Radushkevich were very large at 303 K, but the mean adsorption energy E values were between 0.367 and 3.580 kJ/mol. These values of mean adsorption energy were <8 kJ/mol, which indicated that the adsorption process might have occurred by physical means.

Harkins–Jura isotherm showed small error function values but did not fit the experimental data. Also, BET isotherm did not fit the experimental data due to its large error function values. Flory–Huggins equilibrium constant K_{FH} obtained is ≤190.546 at 303–333 K (see Table 5).

The adsorption capacities of some adsorbents for Cr(III), compared to MNB, are depicted in Table 6. The adsorption capacity of MNB for Cr(III) showed that it demonstrated a potential of being utilised as adsorbent for the removal of toxic Cr(III) and toxic other metal ions from polluted water.

From thermodynamic standpoint, the values of negative values of ΔG^0 at all temperatures showed the spontaneity and feasibility of the adsorption system. The value of ΔH^0 was obtained as +46.219 kJ/mol, which indicated that the process was endothermic. This supported the increase in adsorption capacity of MNB for Cr(III) from 303-333 K. Also the value of ΔS^0 was obtained as +118.792 J/mol/K,

Table 7 Thermodynamic parameters for Cr(III) uptake by MNB

ΔG^o (kJ/mol)	−12.571
	−8.933
	−9.071
ΔH^o (kJ/mol)	+46.219
ΔS^o (J/K/mol)	+118.792

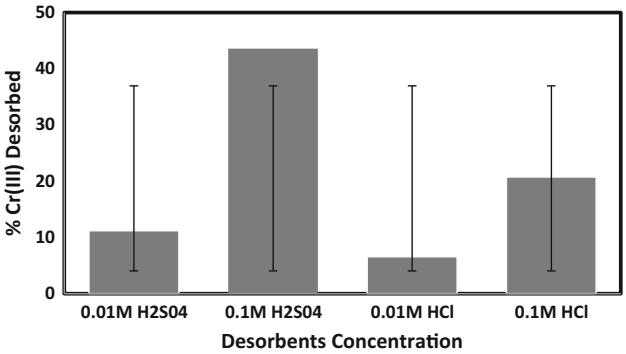

Fig. 4 % Desorption of Cr(III) from MNB using H_2SO_4 and HCl as desorbents

Table 6 The adsorption capacities of different materials for Cr(III) Ions

Materials	Adsorption capacities (mg/g)	References
Termitomyces clypeatus	24.84	Fathima et al. (2015)
Immature coal (Leonardite)	75.20	Lao-Luque et al. (2014)
Bacillus subtilis	23.90	Aravindhan et al. (2012)
Titanate whiskers	97.00	Hang et al. (2014)
Sargassum cymosum	98.80	De Souza et al. (2013)
Sugarcane biochar	15.83	Xiong et al. (2013)
Sugarcane pulp residue	3.43	Xiong et al. (2013)
Parkia biglobosa chaff	170.07	Ogbodu et al. (2015)
Parkia biglobosa pulp	324.68	Ogbodu et al. (2015)
Chitosan polymer	41.50	Zuo and Balasubramanian (2013)
MnO_2 nano-bioextractant	5.82	This study

which indicated an increase in the degree of randomness of the process (see Table 7).

The thermodynamic result further showed that the adsorption processes would be better supported at elevated temperatures. This corroborates the result of separation factor that was obtained from Langmuir isotherm. In other words, endothermicity is a driving force that will increases the mass transfer of Cr(III) solute from the bulk solution phase to surface of the adsorbent, before the intraparticle and pore diffusion processes take place (Kumar et al. 2009).

Desorption studies

Desorption studies are done to know the amount of adsorbents that can be regenerated or recycled when put to pragmatic use. The cost effectiveness and economics of adsorbents are their abilities to be regenerated after use over time. For the Cr(III)-loaded MNB, 0.01 and 0.1 M H_2SO_4 desorbed 11.18 and 43.53 % of Cr(III) adsorbed, respectively, while 0.01 and 0.1 M HCl desorbed 4.9 and 16.86 % of Cr(III) adsorbed, respectively. Figure 4 shows the % Cr(III) desorbed at different concentrations of desorbents. From this result, it was observed that 0.1 M H_2SO_4 and 0.1 M HCl desorbed Cr(III) better than 0.01 M H_2SO_4 and 0.01 M HCl. Although the percentage Cr(III) desorption by the two desorbents was not high as anticipated, the material still showed a good potential of being used industrially.

Conclusion

Competitive adsorption modelling of Cr(III) from single and binary aqueous solutions was examined. The experimental data obtained were fitted into various mathematical models. Pseudo-second-order and Langmuir models fit the experimental data best.

Desorption study showed that MNB can be regenerated and reused as adsorbent for the treatment of water, wastewaters and industrial wastewaters polluted with Cr(III) and Cr(III) in the presence of other micro-pollutants (that is under competitive condition).

Acknowledgments The authors acknowledge the support of The World Academy of Sciences—for the advancement of science in developing countries (TWAS), Italy and the Chinese Academy of Sciences (CAS), China for providing Fellowship (*FR Number: 3240240234*) to Dr Martins O. Omorogie at the Laboratory for Nanodevices of the National Center for Nanoscience and Technology, Beijing, China where this research was done. This work was also supported in part by the National Basic Research Program of China (973 Program No. 2011CB933401) and the National Natural Science Foundation of China (21005023). Prof. Jian R. Gong gratefully acknowledges the support of the K.C. Wong Education Foundation, Hong Kong.

Compliance with Ethical Standards

Conflict of interest The authors declare that there is no conflict of interest.

References

Abbas M, Nadeem R, Zafar MN, Arshad M (2008) Biosorption of chromium (III) and chromium (VI) by untreated and pretreated *Cassia fistula* biomass from aqueous solutions. Water Air Soil Pollut 191:139–148

Adeoye AO, Waigh RD (1983) Secoiridoid and Triterpenic acids from the stems of *Nauclea diderrichii*. Phytochemistry 22(4): 975–978

Aguado J, Arsuaga JM, Arencibia A, Lindo M, Gascon V (2009) Aqueous heavy metals removal by adsorption on amine-functionalised mesoporous silica. J Hazard Mater 163:213–221

Aravindhan R, Fathima A, Selvamuru M (2012) Adsorption, desorption, and kinetic study on Cr(III) removal from aqueous solution using *Bacillus subtilis* biomass. Clean Technol Environ Policy 14(4):727–735

Barrera H, Urena-Nunez F, Bilyeu B, Barrera-Diaz C (2006) Removal of chromium and toxic ions present in mine drainage by *Ectodermis Opuntia*. J Hazard Mater B136:846–853

Bayramoğlu G, Arica MY (2008) Adsorption of Cr(VI) onto PEI immobilised acrylate-based magnetic beads: isotherms, kinetics and thermodynamics study. Chem Eng J 20:20–28

Brunauer S, Emmett PH, Teller E (1938) Adsorption of gases in multi-molecular layers. J Am Chem Soc 60:309–319

Byrappa K, Yoshimura M (2001) Handbook of hydrothermal technology. Noyes Publications, New York

Chen T, Wise SS, Kraus S, Shaffiey F, Wise Dr JP (2009) Particulate hexavalent chromium is cytotoxic and genotoxic to the north atlantic right Whale (*Eubalaena glacialis*) lung and skin fibroblasts. Environ Mol Mutagen 50:387–394

Cimino G, Passerini A, Toscano G (2000) Removal of toxic cations and Cr (VI) from aqueous solution by hazelnut shell. Water Res 34:2955–2962

De Souza FB, Ulson Guelli, de Souza SMA, Ulson de Souza AA, Costa CAE, Botelho CMS, Vilar VJP, Boaventura RAR (2013) Modeling of trivalent chromium speciation in binding sites of marine macroalgae *Sargassum cymosum*. Clean Technol Environ Policy 15(6):987–997

Dubinin MM (1960) The potential theory of adsorption of gases and vapors for adsorbents with energetically non-uniform surface. Chem Rev 60:235–266

Elangovan R, Philip L, Chandraraj K (2008) Biosorption of hexavalent and trivalent chromium by palm flower (*Borassus aethiopum*). Chem Eng J 141:99–111

Fathima A, Aravindhan R, Rao JR (2015) Biomass of *Termitomyces clypeatus* for chromium(III) removal from chrome tanning wastewater. Clean Technol Environ Policy 17(2):541–547

Freundlich HMF (1906) Over the adsorption in solution. J Phys Chem 57(1906):385–390

Garcia-Reyes RB, Rangel-Mendez JR (2010) Adsorption kinetics of chromium(III) ions on agro-waste materials. Bioresour Technol 101:8099–8108

Gerente C, Lee VKC, Le Cloirec P, Mckay G (2007) Application of chitosan for the removal of metals from wastewaters by adsorption-mechanisms and models review. Critical Rev Environ Sci Technol 37:41–127

Granados-Correa F, Corral-Capulina NG, Olguín MT, Acosta-León CE (2011) Comparison of the Cd(II) adsorption processes

between boehmite (γ-AlOOH) and goethite (α-FeOOH). Chem Eng J 171:1027–1034
Hang Y, Yin H, Wang A (2014) Preparation of titanate whiskers starting from metatitanic acid and their adsorption performances for Cu(II), Pb(II), and Cr(III) ions. Water Air Soil Pollut 225:2095–2108
Harkins WD, Jura CJ (1944) Surfaces of solids XIII; A vapor adsorption method for the determination of the area of a solid without the assumption of a molecular area, and the areas occupied by nitrogen and other molecules on the surface of a solid. J Am Chem Soc 66:1366–1373
Ho Y. S (1995) Adsorption of heavy metals from waste streams by peat. Ph.D. Thesis, University of Birmingham, Birmingham
Ho Y-S, Chiang T-H, Hsueh Y-M (2005) Removal of basic dye from aqueous solution using tree fern as a biosorbent. Proc Biochem 40:119–124
Horsfall M, Spiff AI (2005) Equilibrium sorption study of Al3+, Co2+ and Ag2+ in aqueous solutions by fluted pumpkin (Telfairia occidentalis HOOK) waste biomass. Acta Chim Slov 52(2005):174–181
Jacobs AJ, Testa SM (2004) Overview of Chromium(VI) in the environment: background and history. In: Guertin J, Jacobs AJ, Jacobs CP (eds) Chromium(VI) handbook. CRC Press Inc, Boca Raton
Johnson BB (1990) Effect of pH, temperature, and concentration on the adsorption of cadmium on goethite. Environ Sci Technol 24:112–118
Kiran S, Kumar AJ, Sinha TJM, Shalini S (2014) Functionalization of nanocrystalline cellulose for decontamination of Cr(III) and Cr(VI) from aqueous system: computational modeling approach. Clean Technol Environ Policy 16(6):1179–1191
Kumar E, Bhatnagar A, Ji M, Jung W, Lee S-H, Kim S-J, Lee G, Song H, Choi JY, Yang JS, Jeon BH (2009) Defluoridation from aqueous solutions by granular ferric hydroxide (GFH). Water Res 43(2):490–498
Ĺopez-Ťellez G, Barrera-Díaz CE, Balderas-Herńandez P, Roa-Morales G, Bilyeu B (2011) Removal of hexavalent chromium in aquatic solutions by iron nanoparticles embedded in orange peel pith. Chem Eng J 173(2):480–485
Langmuir I (1916) The adsorption of gases on plane surfaces of glass, mica and platinum. J Am Chem Soc 40:1361–1403
Lao-Luque C, Solé M, Gamisans X (2014) Characterization of chromium (III) removal from aqueous solutions by an immature coal (leonardite); Toward a better understanding of the phenomena involved. Clean Technol Environ Policy 16(1):127–136
Li Q, Zhai J, Zhang W, Wang M, Zhou J (2007) Kinetic studies of adsorption of Pb(II), Cr(III) and Cu(II) from aqueous solution by sawdust and modified peanut husk. J Hazard Mater 141:163–167
Li J, Lin Q, Zhang X, Yan Y (2009) Kinetic parameters and mechanisms of the batch biosorption of Cr(VI) and Cr(III) onto *Leersia hexandra* Swartz biomass. J. Col. Interf Sci 333:71–77
Lisha KP, Maliyekkal SM, Pradeep T (2010) Manganese dioxide nanowhiskers: a potential adsorbent for the removal of Hg(II) from water. Chem Eng J 160:432–439
Lorenc-Grabowska E, Gryglewicz G (2005) Adsorption of lignite-derived humic acids on coal-based mesoporous activated carbons. J. Colloid Interf Sci 248:416–421
Melitas N, Chuffe-Moscoso O, Farrell J (2001) Kinetics of soluble chromium removal from contaminated water by zerovalent iron media: corrosion inhibition and passive oxide effects. Environ Sci Technol 35:3948–3953
Mobasherpour I, Salahi E, Pazouki M (2012) Comparative of the removal of Pb^{2+}, Cd^{2+} and Ni^{2+} by nanocrystallite hydroxyapatite from aqueous solutions: adsorption isotherm study. Arabian J Chem 5(2012):439–446
Ofomaja AE, Naidoo EB, Modise SJ (2009) Removal of copper(II) from aqueous solution by pine and base modified pine cone powder as biosorbent. J Hazard Mater 168:909–917
Ogbodu RO, Omorogie MO, Unuabonah EI, Babalola JO (2015) Biosorption of heavy metals from aqueous solutions by *Parkia biglobosa* biomass: equilibrium, kinetics, and thermodynamic studies. Environ Prog Sustainable Energy. doi:10.1002/ep.12175
Oliveira EA, Montanher SF, Andrade AD, Nobrega JA, Rollemberg MC (2005) Equilibrium studies for the sorption of chromium and nickel from aqueous solutions using raw rice bran. Proc Biochem 40:3485–3490
Omorogie MO, Babalola JO, Babalola EI, Song W, Gong JR (2012) Efficient chromium abstraction from aqueous solution using a low-cost biosorbent: *Nauclea diderrichii* seed biomass waste. J Saudi Chem Soc. doi:10.1016/j.jscs.2012.09.017
Onal Y, Akmil-Basar C, Sarici-Ozdemir C (2007) Investigation kinetics mechanisms of adsorption malachite green onto activated carbon. J Hazard Mater B146:149–203
Oszlanczi G (2011) Nervous system effects and oxidative stress in rats treated with metal oxide nanoparticles. PhD Thesis, University of Szeged, Hungary
Posselt HS, Anderson FJ, Walter WJ (1968) Cation sorption on colloidal hydrous manganese dioxide. Environ Sci Technol 2:1087–1093
Rodríguez-Martínez CE, González-Acevedo ZI, Olguín MT, Frías-Palos H (2015) Adsorption and desorption of selenium by two non-living biomasses of aquatic weeds at dynamic conditions. Clean Technol Environ Policy. doi:10.1007/s10098-015-0987-9
Romero-Gonzalez J, Gardea-Torresdey JL, Peralta-Videa JR, Rodriguez E (2005) Determination of equilibrium and kinetic parameters of the adsorption of Cr(III) and Cr(VI) from aqueous solutions to *Agave Lechuguilla* biomass. Bioinorg Chem Appl 3:55–68
Şahan T, Öztürk D (2014) Investigation of Pb(II) adsorption onto pumice samples: application of optimization method based on fractional factorial design and response surface methodology. Clean Technol Environ Policy 16(5):819–831
Sawalha MF, Peralta-Videa JR, Romero-Gonzalez J, Gardea-Torresdey JL (2006) Biosorption of Cd (II), Cr(III), and Cr(VI) by saltbush (*Atriplex canescens*) biomass: thermodynamic and isotherm studies. J. Colloid Interf Sci 300:100–104
Sevim AM, Hojiyev R, Gül A, Çelik MS (2011) An investigation of the kinetics and thermodynamics of the adsorption of a cationic cobalt porphyrazine onto sepiolite. Dyes Pigm 88:25–38
Shi W, Tao S, Yu Y, Wang Y, Ma W (2011) High performance adsorbents based on hierarchically porous silica for purifying multicomponent wastewater. J Mater Chem 21(39):15567–15574
Stumm W, Morgan JJ (1996) Aquatic chemistry, 3rd edn. Wiley, New York
Subramanian V, Zhu H, Wei B (2008) Alcohol-assisted room temperature synthesis of different nanostructured manganese oxides and their pseudo-capacitance properties in neutral electrolytes. Chem Phys Lett 453:242–249
Temkin M, Pyzchev V (1939) Kinetics of the synthesis of ammonia on promoted iron catalyst. J Phys Chem 13:851–855
The International for Conservation of Nature (IUCN) (1998) African regional workshop. Conservation and Sustainable Management of Trees, Harare
Thirumavalavan M, Lai Y-L, Lee J-F (2011) Fourier transform infrared spectroscopic analysis of fruit peels before and after the adsorption of heavy metal ions from aqueous solution. J Chem Eng Data 56:2249–2255
Tripathy SS, Bersillon JL, Gopal K (2006) Adsorption of Cd^{2+} on hydrous manganese dioxide from aqueous solutions. Desalination 194:11–21

Tsai Y-P, Doong R, Yang J-C, Wu Y-J (2011) Photo-reduction and adsorption in aqueous Cr(VI) solution by titanium dioxide, carbon nanotubes and their composite. J Chem Tech Biotechnol 86:949–956

Venkatesan G, Senthilnathan U, Rajam S (2014) Cadmium removal from aqueous solutions using hybrid eucalyptus wood based activated carbon: adsorption batch studies. Clean Technol Environ Policy 16(1):195–200

Xiong L, Chen C, Chen Q, Ni J (2011) Adsorption of Pb(II) and Cd(II) from aqueous solutions using titanate nanotubes prepared via hydrothermal method. J Hazard Mater 172:68–74

Xiong ZY, Wang S, Li B, Wei-chun QY (2013) Cr(III) adsorption by sugarcane pulp residue and biochar. J. Central South Univ 20(5):1319–1325

Young DM, Crowell AD (1962) Physical adsorption of gases. Butterworth, London

Zou W, Han R, Chen Z, Zhang J, Shi J (2006) Kinetic study of adsorption of Cu(II) and Pb(II) from aqueous solutions using manganese oxide coated zeolite in batch mode. Colloid Surf A 279:238–246

Zubair A, Bhatti HN, Hanif MA, Shafqat F (2008) Kinetic and equilibrium modeling for Cr(III) and Cr(VI) removal from aqueous solutions by *Citrus reticulata* waste biomass. Water Air Soil Pollut 191:305–318

Zuo X, Balasubramanian R (2013) Evaluation of a novel chitosan polymer based adsorbent for the removal of chromium (III) in aqueous solutions. Carb Polym 92(2):2181–2186